Chapter 1

Quaternary Geochronology Using Accelerator Mass Spectrometry (AMS) – Current Status of the AMS System at the TONO Geoscience Center

Akihiro Matsubara, Yoko Saito-Kokubu,
Akimitsu Nishizawa, Masayasu Miyake,
Tsuneari Ishimaru and Koji Umeda

Additional information is available at the end of the chapter

http://dx.doi.org/10.5772/58549

1. Introduction

1.1. Background

The Tono Geoscience Center (TGC) of the Japan Atomic Energy Agency (JAEA) has been conducting research into the long term (several million years) stability of underground environments, in order to provide the scientific knowledge needed to ensure safety and reliability for the geological disposal of high-level radioactive waste [1–3]. The time scale for occurrence of the relevant geoscientific activities, as shown in Figure 1, i.e., earthquake/fault and volcanic activities, behavior of groundwater flow, uplift/subsidence and erosion of the ground surface, and so on, corresponds well to the duration of the Quaternary Period geology. Geochronology of the Quaternary Period has been strongly enhanced by measurement of terrestrial *in situ* cosmogenic radionuclides, such as ^{10}Be, ^{14}C, ^{26}Al, and ^{36}Cl, produced by secondary cosmic rays (e.g., neutron, muon) which are generated by interaction between the atmosphere of earth and primary cosmic rays that originate from the sun and galactic systems.

Applications of accelerator mass spectrometry (AMS) using those rare radionuclides for geological studies have been summarized by various authors [4–7]. It is a well-known fact that ^{14}C has been widely utilized in several disciplines, including geology, environmental science, archaeology, and biomedicine. With regard to research into underground geological disposal of waste, radiocarbon dating of organic samples (e.g., bulk organic, humic acid, and humin fractions) taken from faults provide an historical archive of typical conventional applications

to the investigation of seismic activity [7,8]. The dates obtained, combined with other scientific and historical information, help to determine whether or not the fault is a so called "active fault", and to estimate cyclicity of seismic events and probability for serious large fault movements during the post-closure duration of geological disposal.

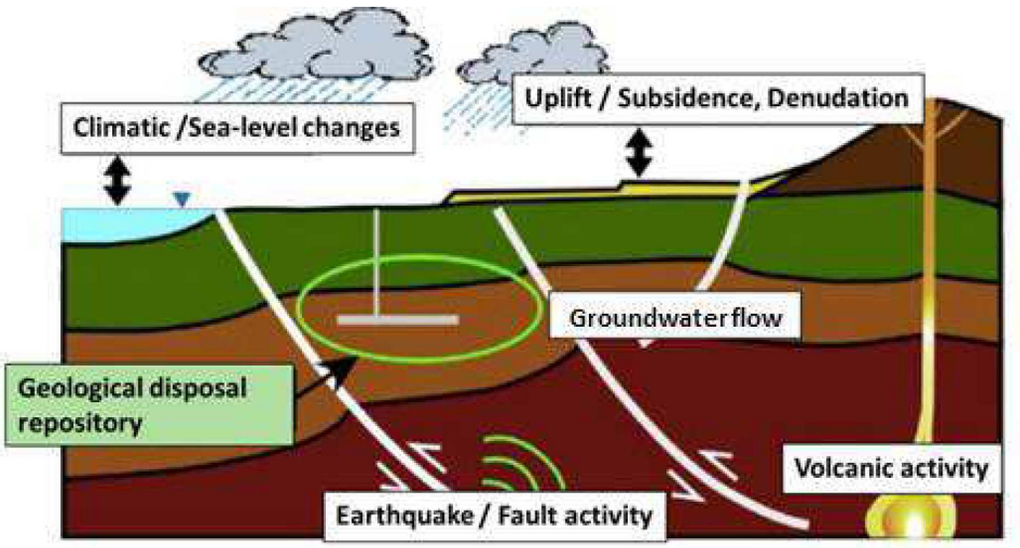

Figure 1. Long-term geological activities relevant to the geological disposal of high-level radioactive waste.

Long-lived cosmogenic radionuclides, such as ^{10}Be, ^{26}Al, and ^{36}Cl enable us to apply to the exposure dating methods on boulder and bedrock surfaces for exposure ages up to 10^7 years [4–7]. These methods can provide information relevant to geological disposal with respect to geomorphological evolution, i.e., erosion rates of rock surfaces, burial histories of rock surfaces and sediments, fault slip rates, and so on. One of the typical radionuclides for surface exposure dating is ^{10}Be, or both ^{10}Be and ^{26}Al. The half-lives of ^{10}Be and ^{26}Al are long enough (1.6 Myr and 0.7 Myr, respectively) to span the entire Quaternary timescale. They can be produced simultaneously in a single sample of quartz where ^{26}Al and ^{10}Be are mainly produced through nuclear spallation from ^{28}Si and ^{16}O, respectively. Concentration of each depends on balance between *in situ* production and surface erosion and generally, there are two unknown variables. The simultaneous measurement of ^{26}Al and ^{10}Be concentration has the advantage of solving for the two variables: exposure age and erosion rate. On the other hand, ^{36}Cl is produced through multi-channel reactions: spallation on Ca and K with neutron and muon, and the thermal neutron capture on ^{35}Cl. This feature provides an advantage to the ^{36}Cl exposure dating that is not restricted to specific rock types or minerals (such as carbonates or silicates) under a number of conditions. Furthermore, decomposition of contribution for ^{36}Cl production into spallogenic, mugenic, and thermal neutron can increase the amount of information for one sample, with the potential for greater erosion-exposure history accuracy.

The measurement of ^{14}C and ^{36}Cl is also applicable to hydrogeologic investigations: studies of groundwater age, origin and mixing. Most of these nuclides are produced through interaction

http://dx.doi.org/10.5772/58549

with alpha-particle/neutron emitted from radioactive elements such as Th and U within the sediment or rock dozens of meters or more underground, where there is no cosmogenic radionuclide production [5].

1.2. Purpose and contents of this article

Our ongoing efforts, therefore, have been dedicated to development of a multi-nuclide AMS for measurement of the rare radionuclides ^{10}Be, ^{14}C, ^{26}Al, and ^{36}Cl. In this article, the current status of the AMS system at the JAEA-AMS-TONO and our activities leading to development of a multi-nuclide AMS are presented.

The next section shows the history and present-day status of our AMS system. The detail of the AMS system and its configuration are described in Section 3. The current status for ^{14}C, ^{10}Be and ^{26}Al measurements is presented in Sections 4, 5, and 6, respectively. Section 7 provides the research and development related to improvement of the isobar discrimination for the ionization chamber. Finally, Section 8 presents a summary.

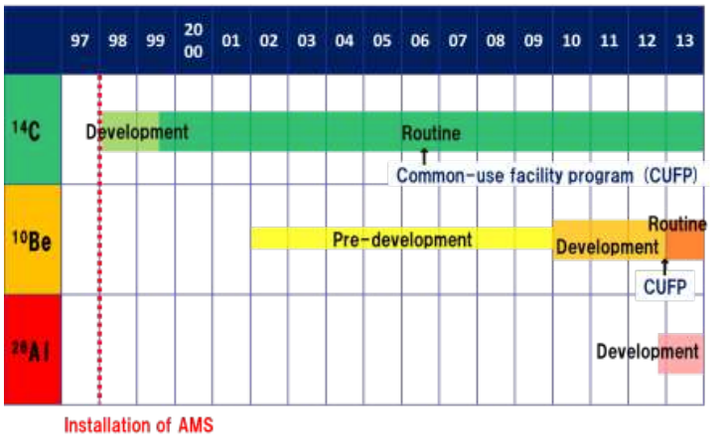

Figure 2. Timeline of the JAEA-AMS-TONO development.

2. Operation status

The history of the JAEA AMS system is depicted in Figure 2. The AMS system was installed at TGC in 1997, and routine measurement of ^{14}C started in 1998 [9]. The preliminary development of the ^{10}Be-AMS started around 2002 [10], intensive development was implemented from 2010 to 2012 [11,12], and progress of which will be described in Section 5. After that, the routine measurement of ^{10}Be started at the beginning of fiscal year 2013. At present, we have initiated the development of the ^{26}Al-AMS (described in Section 6) [13, 14]. Furthermore, as a part of preparatory activity for the development of the ^{36}Cl-AMS, we have started to investigate the nature of the pulse trace that is disturbed by interfering particles in the heavy ion detector, in order to improve the discrimination performance for the detector system (presented in Section 7) [15].

The evolutions of the measurement time and the number of sample cathode (target) are shown in Figure 3. Total, cumulative, measurement time (the blue line) has increased more or less continuously for 15 years, and reached 15,000 hours this fiscal year. Around 2005, routine measurements ceased for a while due to system maintenance by the lab-staff. As shown on the bar chart, the average number of samples measured annually is between 800 and 1000, and the total number of samples will exceed 12,500 within the next few months. After the development of the ^{10}Be measurement has been intensive since the start, the proportion of ^{10}Be samples to the total sample number has increased rapidly. In fiscal year 2012, the proportion of ^{14}C, ^{10}Be and ^{26}Al sample cathodes are 76%, 20%, and 4%, respectively.

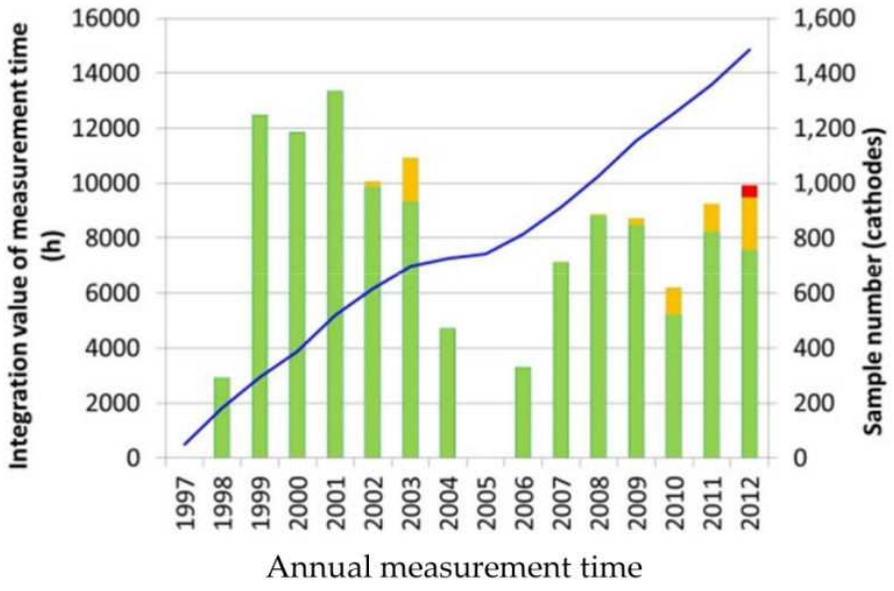

Figure 3. Evolution of the measurement time and sample number.

In Figure 4, the pie chart on the left shows the proportion of ^{14}C-AMS samples measured for the various study fields in fiscal year 2012. Geoscience accounted for about 60%, while environmental studies accounted for most of the balance. The proportion labeled as "Analysis" stands for the cathode number used in our technical development. The pie chart on the right in Figure 4 illustrates the relative proportion of measured samples requested by users in JAEA to other users. Almost all of the samples were requested by JAEA users. The measurement of the other samples were performed under JAEA's common-use facility program for non-JAEA users [16]. This program started in 2006, in order to enlarge and expand the public use of JAEA's facilities. The study fields using the program were mostly in environmental science and archaeology.

http://dx.doi.org/10.5772/58549

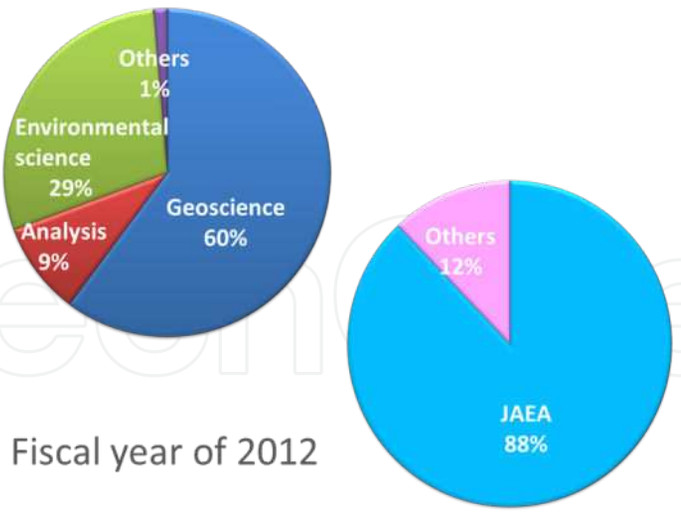

Figure 4. Proportion of ^{14}C-AMS samples measured in the various investigation fields (left) and, on the right, those requested by JAEA users to by others in fiscal year 2012.

3. AMS system

3.1. Overall features

The AMS system is a versatile system based on the Pelletron™ tandem accelerator (Model 15SDH-2, 5 MV terminal voltage) [17]. The same type (5 MV Pelletron) of the AMS system has been used in other facilities, for example, at the Micro Analysis Laboratory, Tandem accelerator (MALT) at the University of Tokyo, Japan [18], the AMS system at the National Institute for Environmental Studies (NIES) of Japan [19], at the Scottish Universities Environmental Research Center (SUERC) in the United Kingdom [20,21], and at the Uppsala 5 MV Pelletron tandem accelerator developed in the Uppsala University, Sweden [22,23].

This AMS system is designed for the AMS analysis with most radio-isotopes including ^{10}Be, ^{14}C, ^{26}Al, ^{36}Cl, and ^{129}I. Although technological advances in recent years have enabled practical use of compact AMS systems below 1 MV allowing the measurement of ^{10}Be, ^{14}C, and ^{26}Al [24–26], the relatively wide range of high terminal voltage greater than several megavolts has, even now, been generally recognized to be beneficial to efficient suppression of signal background, resulting in further potential for expandability for a multi-nuclides measurement.

3.2. System description [17]

Figure 5 is a schematic of the AMS system layout. The system can be divided into five major subsystems: the ion sources, the sequential injection system, the tandem Pelletron accelerator, the post-accelerator beamline with the high-energy mass spectrometer components, and the heavy ion detection system by means of the ionization chamber. There are eight vacuum turbomolecular pumping systems attached along the beamline, where, several beam steerers

and magnetic or electrostatic lenses are located, and the total length of the system is around 31 metres. Summary of the system configuration for rare isotopes are presented individually in Table 1.

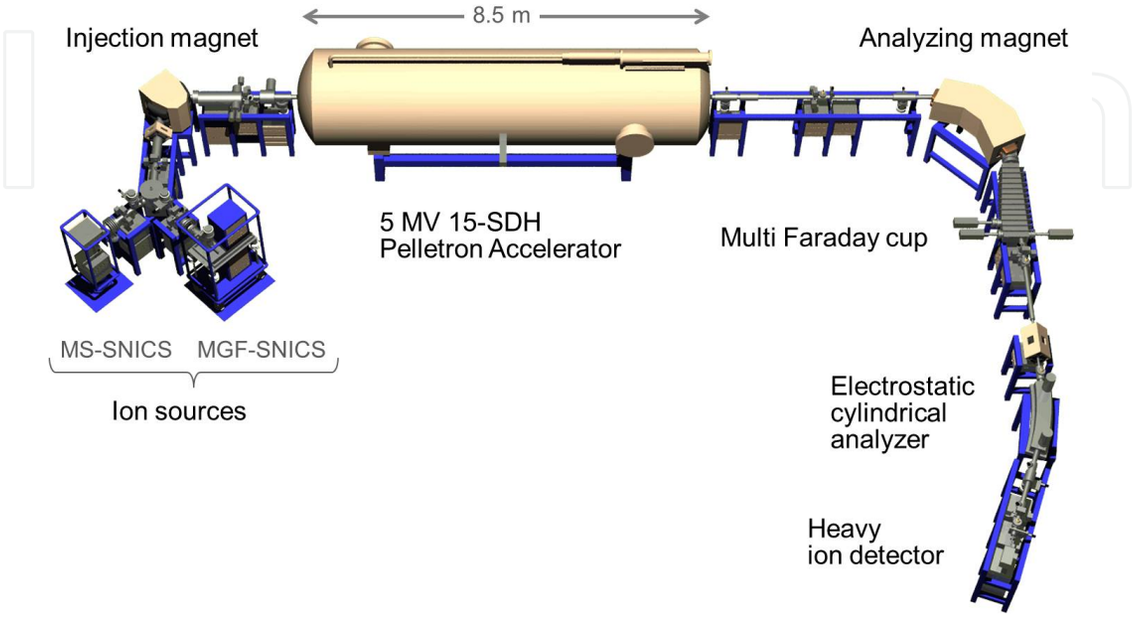

Figure 5. AMS system at JAEA-AMS-TONO.

Nuclide	^{14}C	^{10}Be	^{26}Al
Terminal volt. (Tot. Energy)	4.5 MV (22.5 MeV)	4.8 MV (16.3 MeV)	4.3 MV (17.2 MeV)
Target	Graphite with Fe powder	BeO with Nb powder	Al_2O_3 with Ag powder
Current	20 μA (C^-)	2 μA (BeO^-)	0.1 μA (Al^-)
Injection	Sequential (^{12}C: 0.3 ms , ^{13}C: 0.9 ms, ^{14}C: 98.6 ms)	Simultaneous ($^{10}Be^{16}O$, $^{9}Be^{17}O$)	Sequential (^{26}Al: 98 ms, ^{27}Al: 1 ms)
Transmit.	58% (^{12}C)	21% (^{9}Be)	39% (^{27}Al)
Meas. ratio (Count rate)	$^{14}C^{4+}/^{12}C^{4+}$, $^{13}C^{4+}/^{12}C^{4+}$ (60 cps@ HOxII)	$^{10}Be^{3+}/^{17}O^{5+}$ (70 cps @S5-1)	$^{26}Al^{3+}/^{27}Al^{3+}$ (15 cps @S4-1)
Background	< 7x10^{-16} (< 0.06 pMC) @WAKO Powder	< 7 x 10^{-15} @MITSUWA powder	< 3 x 10^{-14} @Blank†
Ionization chamber	ΔE_1-E_{Res}	ΔE_1-E_{Res} (with gas cell)	ΔE_1-E_{Tot}

† Sample of BLK was made from a quantified standard sample for atomic absorption spectrometry supplied from Wako Pure Chemical Industries, Ltd.

Table 1. Summary of current AMS specifications for the JAEA-AMS-TONO.

http://dx.doi.org/10.5772/58549

The ion sources, the Multi-Cathode, Source of Negative Ions by Cesium Sputtering (MC-SNICS) for solid samples (40 cathodes) and the Multiple Gas Feed, SNICS (MGF-SNICS) for CO_2-gas samples (12 cathodes) are connected to the main beamline through the 45° electrostatic spherical analyzer (ESA). The sources consist of a cesium oven generating Cs vapour, a heated ionizer electrode producing a focused Cs^+ beam at the sample cathode, and extraction and focus electrodes. Particles sputtered from the sample cathode by Cs^+ bombardments pick up electrons as they pass through the cesium layer condensed on the sample; thus, negative ions are produced. To stabilize the cesium vapour feed to the source, we added a simple auto-controllable electrical heating subsystem to the cesium oven and its feeder pipe; the standard deviation of the temperature monitored during the routine measurement has been kept within a range of ±0.5C° [27]. This type of simple technical addition or modification is commonly used for the same purpose [28]. The acceleration voltage of the ion source is usually set to 55 kV. By using the beam-slit located at the image point of the ESA (before the injection magnet), the "tail" of the beam profile can be trimmed, where the tail is due to an energy spread in the sputtering process. This trimming assures open-aperture optical properties (often called "flat top transmission") on the downstream side of that slit. The combination of the ESA and the injection magnet ($ME / q^2 \leq 15$, where M is the mass number of the ion, E is the ion energy in MeV and q is the charge number, and the nominal radius is 0.457 m) limits the specific charge-to-mass ratio, M / q, for the transmittance of negative ions in the pre-accelerator region to remove unwanted particles from the ion beam. The mass resolution ($M / \Delta M$) reaches 200 for the electrostatic and magnetic filters combination. The same concept is applied for the high-energy post-accelerator region containing the analyzing magnet and electrostatic cylindrical analyzer (ECA) listed below.

The AMS system employs the sequential injection method for the precise measurement of the ratio of rare to abundant isotopes regardless of fluctuations of source conditions. This method, or the rapid switching of the masses (isotopes) to be injected toward the accelerator, (so called sequence "bounced" or "jumping" beams) is accomplished by applying an appropriate bias potential to the electrically insulated bent chamber inside the injection magnet. Most of the duration (~99%) in the sequential injection is allocated for the measurement of the rare isotope (details in Table 1).

In the tandem Pelletron accelerator (15-SDH), there are two parallel chains charging the high-voltage terminal with current up to 300 μA. The consequent maximum terminal potential of 5 MV leads to the suitable stripped ionization state of 4+ for carbon by using a gas stripper (the ion beam energy is up to 25 MeV). For the chlorine, the charge state is designed to be 7+ or 8+ by using a foil stripper and its energy would be lie in the range of 42-45 MeV. The pressure of the stripper gas is typically 10 μTorr, 9 μTorr, and 5 μTorr for ^{14}C-, ^{10}Be-, and ^{26}Al-measurement, respectively.

The high-energy mass spectrometer in the post-accelerator region is composed of magnetic and electrostatic filters and detector systems. The analyzing magnet (produced by Danfysik A/S) is a double focusing 90° sector magnet with a nominal radius of 1.270 m, having parameters of $ME / q^2 \leq 176$ and $M / \Delta M$=725. After the off-axis, multi-Faraday cup detector for the abundant isotopes, the 20° ECA with a nominal radius of 3.810 m is used to remove abundant

isotopes having the same mass energy product as the rare isotopes. The resolution attained by the ECA is $M/\Delta M$=200.

The final detector for counting the rare isotopes, the "heavy ion detector", is the gas ionization detector that contains multiple ΔE electrodes (five) arranged along the axis of the beamline (for details see Section 5.2). A nearly equivalent type of detector is used at the SUERC facility in the UK [21]. The ΔE electrodes determine the specific of energy loss arising in their respective regions. In the case for the ion energy over MeV/u, the rate of the energy loss (or stopping power) increases with increasing atomic number. Thus, the spectrum on the plane given by energy-loss 2D-coordinates for various combinations of ΔE electrodes shows its characteristic position on that plane, which makes it possible to distinguish the spectrum of desired nuclide from other spectra of interfering particles. Typical particles interfering with the rare isotopes of ^{10}Be, ^{14}C, and ^{36}Cl are respectively ^{10}B, ^{7}Li, and ^{36}S; their M/q ratios can be equivalent to those of the rare isotop es, thus allowing their entry into the detector. The problem with respect to the ^{10}B and ^{36}S is known as an isobar problem (different elements but same atomic weight). The M/q ratio of $^{14}C^{4+}$ coincides with that of $^{7}Li^{2+}$; although the prime number of charge state (3+ for ^{14}C in this case) is preferable to avoid the coincidence of the M/q ratio, we focus on the higher stripping yield for 4+ (59% at 4.5 MV [5]) rather than 3+ (55% at 2.9 MV [5]). Since the relative difference between atomic numbers for the case of "Be and B" or "Cl and S" is much smaller than the difference for C and Li, distinguishing them in the former case is harder than in the latter case. Therefore, discrimination techniques are crucial for measurements of ^{10}Be and ^{36}Cl. A gas absorber technique has been employed in the ^{10}Be-AMS operation, which is described in Section 5.2. In addition, investigation of a pulse trace fluctuation caused by interfering particles in a preparation for the ^{36}Cl measurement is presented in Section 7.

4. ^{14}C measurement

4.1. Stability and reliability

In the ^{14}C-AMS operation, the stability and reliability of the routine measurements have been checked continuously against measuring standards. The typical standards are, IAEA-C1, -C5, and -C6 [29], and the oxalic acid HOxII (SRM-4990C) that is produced by the National Institute of Standards and Technology, NIST in the USA. Such checks have been performed simultaneously with routine measurements. In our AMS analysis, usually only the HOxII is used for obtaining the normalization constant that is given by the δ^{13}C corrected activity divided by the *fraction modern* for the HOxII (1.3406). Here, the term *fraction modern* is a quantity defined as the ratio of a sample ^{14}C activity A_{SN} to a normalized sample ^{14}C activity A_{ON}, where A_{ON} is equal to the ^{14}C-decay corrected *absolute international standard specific activity* A_{abs} that is intended to correspond to the hypothetical specific activity of atmospheric carbon of year 1950 (in detail see Ref.[30,31]). With respect to data quality of the HOxII standard, therefore, only the relative precision (or relative standard deviation, *rsd*) affects the normalization constant; in other words, the accuracy itself has no meaning. The value of *rsd* for the HOxII is around 0.22% in every routine-measurement. The

http://dx.doi.org/10.5772/58549

procedure of data analysis, as well as ^{10}Be and ^{26}Al analyses has followed an algorithm in the software code "abc" available from the NEC Corporation [30]. It is noted that to obtain the net activity the $^{14}C/^{12}C$ ratio for all samples (except C1) is normally subtracted by the IAEA-C1 value as the chemical background due to the sample preparation, where C1 is made from marble, and its nominal value in the *percent Modern Carbon* (pMC) that is equivalent to the 100%× *fraction modern* (described above) is 0.00 ± 0.02 [29].

The left column of rectangles on Figure 6 shows the evolution of pMC for IAEA-C6, -C5, and -C1 in the year 2013. In some periods no ^{14}C measurements were performed. The period from May to June was allotted for ^{10}Be measurements. Intensive system maintenance was carried out (normally annually) in August, and then ^{10}Be measurements were performed until the end of September. Almost all measured pMC-values for both C6 and C5 are in agreement with the nominal values within 3σ of each point (σ is basically the statistical uncertainty that is inversely proportional to the square root of ^{14}C counts). A few irregular points in C6 could be due to surface roughness of the graphite sample. The roughness is reflected by unsuccessful graphite compression with an Arbor press (hammering with a press-pin). We continue to check the surface condition and data related to such irregular results.

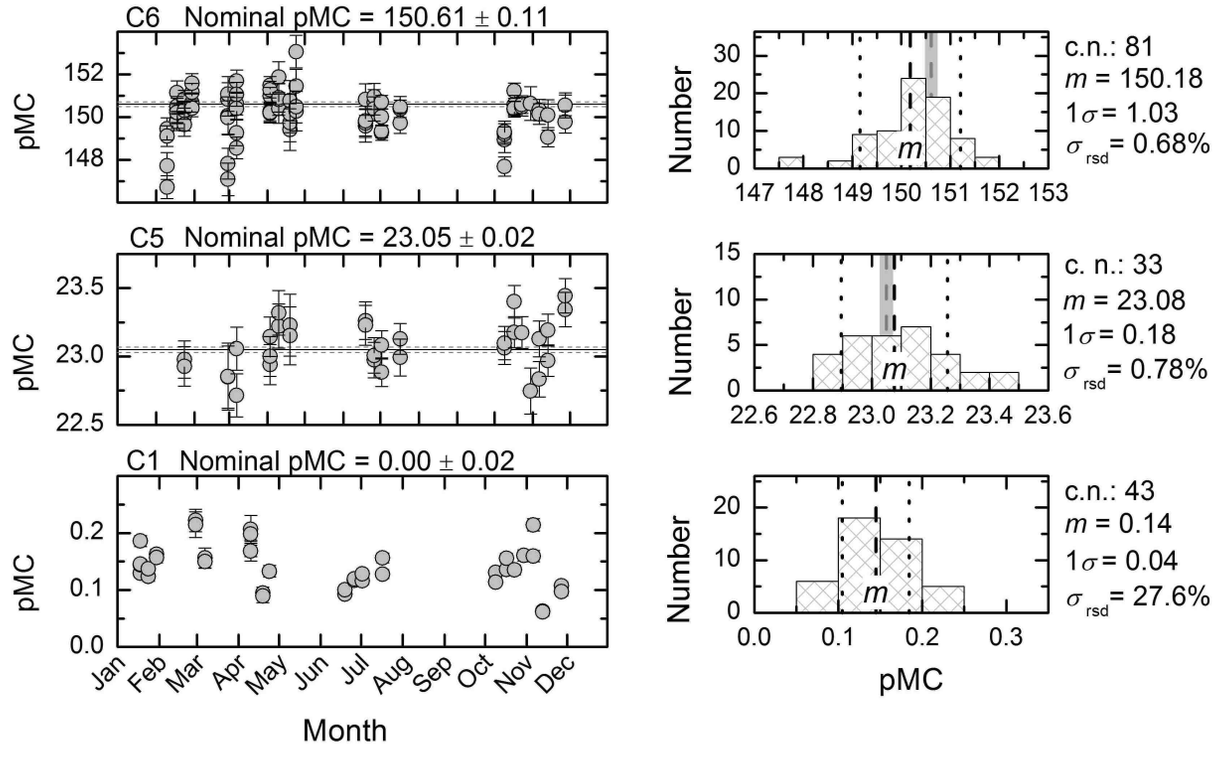

Figure 6. Measurement quality in a 12-month period for ^{14}C-AMS standards: C6 (a), C5 (b), and C1 (c). The left column shows evolutions of the measured value in percent Modern Carbon for the year 2013. The gray line and hatch for both left and right columns depicts respectively the nominal value and its range of uncertainty. The right column shows corresponding histograms for the left column measurement points. The dashed and dotted lines present respectively the arithmetic mean m and its standard deviation σ_H on the histogram. The symbol c.n. stands for the number of sample cathodes used in constructing the histogram, and σ_{Hrsd} is the relative standard deviation given by $\sigma_H/m\times$ 100%.

The frames in the right-hand side of Figure 6 show histograms corresponding to temporal evolution for each standard in the left frames. It can be seen that the arithmetic mean of the histogram for C6 (labelled as *m*) is significantly lower than the range of its nominal value; in other words, a difference between them of 0.36% is quite a bit larger than "the standard deviation of *m*" of 0.10% given by $1\sigma_H/(\text{c.n.})^{0.5}$ where c.n. is the cathode number used in constructing the histogram. This fact, however, is very similar to results obtained in other facilities [32,33], suggesting to us to reconsider use of the nominal value for the purpose of comparisons with measured data. On the other hand, the arithmetic mean for C5 is consistent with its nominal value; the difference between them is within the standard deviation of *m* of 0.03%. The $\pm 1\sigma_H$ (0.18%) of the histogram for C5 is equivalent to ±100 years in its ^{14}C age of 11,750 years, which can be a measure of the confidence interval for one-year. This performance is comparable with the other facilities, e.g., a well-known carbon dating lab in Japan, the Paleo Labo Co.,Ltd [33,34]. For C1, although the arithmetic mean is 0.15 pMC, sometimes values are below 0.1 pMC. This scatter implies possibility of contamination during the sample preparation, which is supported by another fact described as follows. In contrast with C1 in the estimation of background, a high-purity synthetic graphite powder (No.072-03845 Wako Pure Chemical Industries, Ltd, Osaka, Japan) is used as a machine background samples. This powder is made from coke (^{14}C-free), and is directly poured into the cathode hole without any chemical preparations; thus, ^{14}C counts detected with the powder are due to machine background. We have continuously observed around 0.06 pMC for the graphite powder, which shows potential for improvement for lowering the background due to chemical process.

4.2. Inter-laboratory comparison testing

Comparison of the results obtained in different laboratories on the same samples is fundamental to objectively assessing accuracy and system performance. Comparison tests were carried out twice, in 2010 and 2012, with another AMS facility, the JAEA-AMS-MUTSU, of the Aomori Research and Development Center, JAEA [35,36]. This facility has provided high-quality ^{129}I-and ^{14}C-AMSs for environmental science studies, especially for marine transport properties of radio-isotopes, as well as for radiocarbon dating. The typical properties of the AMS system are as follows: a 3 MV Tandetron Cockcroft–Walton accelerator manufactured by High Voltage Engineering Europa, and the simultaneous injection system with the separator-combiner.

In the comparison test performed in 2012, the samples of the HOxII, C5, and C1 were prepared in the MUTSU, distributed to the TONO, and measured in both facilities. The measurement condition such as the duration time or the beam current was taken as the normal condition in each facility. Figure 7 shows results obtained in 2012. For the data analysis, the algorithm used in the TONO was employed. It can be seen for the C5, that there was no significant difference between data obtained in both facilities. The results of the C1 analyzed in the TONO are much lower than that for the MUTSU. This is mostly due to the fact that during ^{14}C counting, ^{13}C ions for the simultaneous injection also entered the accelerator continuously, thus the counting rate (or its possibility) of ^{13}C coming into the ionization detector is much higher for the simultaneous injection than for the sequential injection, in spite of filtering by the combination of magnetic

http://dx.doi.org/10.5772/58549

and electrostatic analyzers. Consequently, the measurement of quite low concentration samples is suitable relative to use by the TONO. The detailed results and discussion for the series of comparison tests will be summarised in a JAEA report in the future.

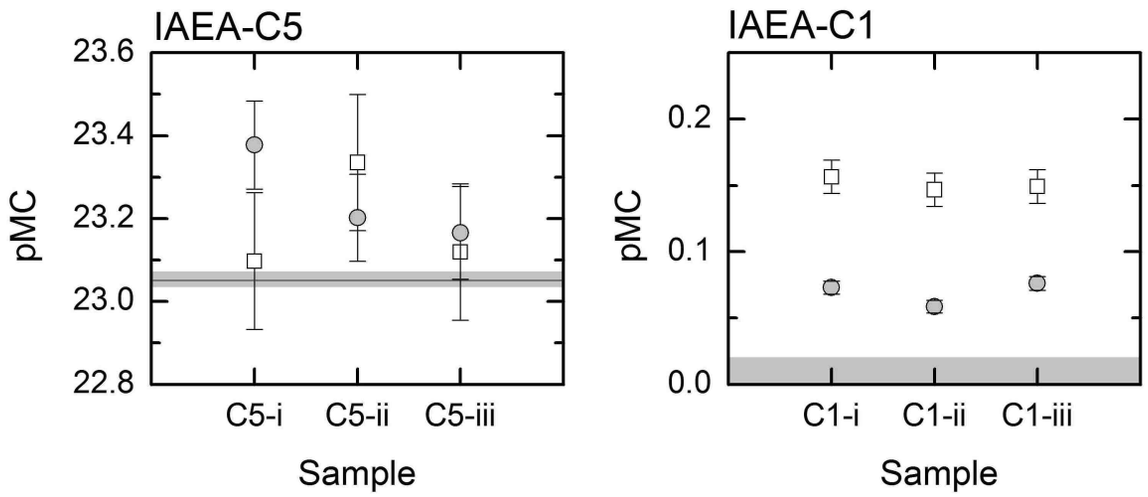

Figure 7. Results of comparison test between JAEA-AMS-TONO (shaded circles) and JAEA-AMS-MUTSU (empty squares). This test was carried out in 2012. The samples were prepared in the MUTSU, distributed to the TONO, and measured in both facilities. The algorithm for the data analysis followed the software code used in the TONO.

5. ^{10}Be measurement

5.1. System configuration and method

The configuration for our ^{10}Be-AMS operation is fundamentally standard, and is based on that used in the MALT [18,37,38]. Samples are made from the solid oxide of beryllium, BeO, for its positive electron affinity to produce negative ions. Since the amount of the rare isotope ^{10}Be is distributed according to the abundance of oxygen isotope ratios, i.e., ^{16}O : ^{17}O : ^{18}O=99.76: 0.04: 0.20, respectively, the ^{10}Be^{16}O is selected for injection into the accelerator to ensure high extraction efficiency of ^{10}Be from the sample. The terminal voltage, usually set at 4.7 or 4.8 MV, is made preferably as high as possible within the range of around 8 MV so as to increase the stripping efficiency from negative ions to 3+ (in our AMS system, the terminal voltage is limited to the specification of 5 MV). In addition, the higher ion energy is also preferred for ensuring the good performance of the discrimination between ^{10}Be and ^{10}B for the heavy ion detector as described below (details in Section 5.2). One of the most significant features of ^{10}Be measurement is the simultaneous injection of ^{9}Be^{17}O with mass the same as ^{10}Be^{16}O for counting the abundance of ^{9}Be isotopes. For this purpose the current of ^{17}O^{5+} is measured to avoid uncertainty in the amount of beryllium hydroxide ^{9}Be^{16}OH contamination in the sample [37]. The abundance isotope is detected with a Faraday cup behind the analyzing magnet as shown in Figure 5.

The mathematical formula used for obtaining the measured isotope ratio (R_m=^{10}Be/^{9}Be) is:

$$R_m = \frac{a_{^{10}Be}}{a_{^{9}Be}} \frac{T_{^{17}O^{5+}}}{T_{^{10}Be^{3+}}} \frac{cps_{^{10}Be^{3+}}}{cps_{^{17}O^{5+}}}, \quad (1)$$

where a is the correction factor for the abundance ratio of the oxygen isotopes, T is transmittance for yielding positive ions from the negative ions, and *cps* is counts per second. The transmittance values for $^{17}O^{5+}$ and $^{10}Be^{3+}$ are substituted by the values for $^{16}O^{5+}$ (=21%) and $^{10}Be^{3+}$ (=6%), respectively. The absolute isotope ratio, R_A, is obtained by correcting the measured ratio, as $R_A=R_m/Const$, where *Const* is the normalization constant that is given by the measured ratio of a standard divided by its nominal ratio. For the ^{10}Be standard, usually so-called "ICN standard 01-5-1" (hereinafter simply S5-1) is used. The series of ICN standards has been prepared and distributed by Nishiizumi of U of C, Berkeley to worldwide AMS laboratories [39].

The boron ions $^{10}B^{3+}$ has the same charge-to-mass ratios as the $^{10}Be^{3+}$, thus it remains on the beamline regardless of the magnetic and electrostatic filters, and results in the entry into the ionization chamber, with respect to the isobar problem as mentioned in Section 3. Usually a gas or solid absorber technique has been used to discriminate between them. Therefore, optimization of the absorber is fundamental in the ^{10}Be measurement.

5.2. Optimization of the rare isotope detector

For the development of the ^{10}Be-AMS, discrimination between the ^{10}Be and ^{10}B isotopes was accomplished by optimization of gas pressures in the ionization chamber and the absorber gas cell (hereinafter simply the gas-cell) attached in front of gas ionization chamber. Figure 8 shows the configuration of the rare isotope detector for the ^{10}Be-AMS in our system. Ionization chamber consists of the cathode electrode (plate), grid, and anodes that are multiple (five) ΔE electrodes arranged along the axis of the beamline. The grid so called *Frisch grid* is to remove the dependence of the pulse amplitude on position of ion pair generation by ionization due to an incident particles.

As mentioned in Section 3.2, the ΔE electrode provides the pulse signal equivalent to the energy loss arising in the area corresponding to the electrode. For incident ion energy over a million electron volts, the rate of energy loss depends largely on the atomic number. Thus, the spectrum peak on the plane given by, e.g., both the coordinates ΔE_1 and E_{Res} (where "Res" means *residual*, see Figure 8) takes a characteristic position on that plane. This individuality of the peak position helps to discriminate the ^{10}B. However, the amount of ^{10}B entering into the ionization chamber is enormous (over 10^6 times larger than that of the ^{10}Be [40]), so that the ^{10}Be signal is disturbed if there is no additional absorber for it. The gas-cell method is an absorbance technique for ^{10}B based on the fact that the energy loss rate for the boron is expected to be larger than that for beryllium for the dependence of energy-loss rate on the atomic number. In our system, the gas-cell is prepared with 1-inch diameter pipe covered by the Havar and Mylar foils at both ends. The nitrogen gas pressure in the absorber significantly affects the shape of the ^{10}Be spectrum, as described below.

http://dx.doi.org/10.5772/58549

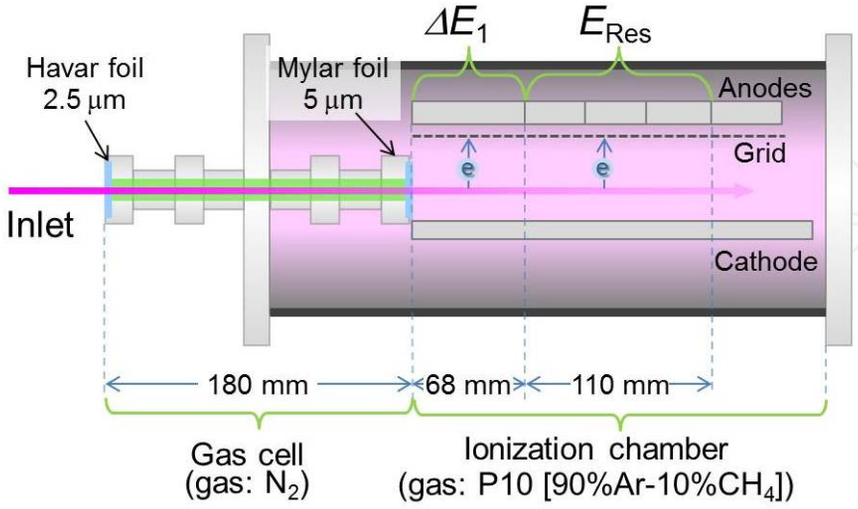

Figure 8. Configuration of the rare isotope detector (heavy ion detector) for ^{10}Be-AMS. The absorber gas-cell is attached in front of ionization chamber. The anode electrode is separated into multiple (five) ΔE electrodes. ΔE_1 and E_{Res} (that means *Residual energy*) indicate the energy loss arising in the region corresponding to the anode plate 1 and plates 2-4, respectively.

We investigated experimentally the discrimination function of the detector system through observation of the variation of the ΔE_1-E_{Res} spectrum by varying the gas pressure of the gas cell. Figure 9 shows the effect of gas pressure on the ΔE_1-E_{Res} spectrum. It can be seen that the horizontal width (ΔE_1 component) is reduced significantly with increasing P_C. It should be noted that the gas pressure of the ionization chamber P_I is decreased with increasing P_C, so as to balance between pulse heights for ΔE_1 and E_{Res}, because the peak position on the Bragg curve (that provides the distribution of energy-loss rate as a function of the distance along the beam axis) shifts toward the gas-cell, as P_c is increased. There is a lower limit of 0.2 V in E_{Res} for data points. This is because the both pulse heights corresponding to (ΔE_1, E_{Res}) coordinates of data points is acquired if the electrical voltage of the E_{Res}-trace exceeds 0.2 V to discriminate between signal and noise. The middle and bottom frames in Figure 9 show the peak profiles in the ΔE_1 component for ^{10}Be and ^{10}B, respectively. These peak profiles are well fitted with the Gaussian curve characterized by the standard deviation of σ_{10Be} and σ_{10B}.

The width of the ^{10}Be peak defined by σ_{10Be} is approximately 1/6 smaller at P_C=58 Torr than that at 32 Torr. As a measure of the discrimination function, the dimensionless normalized distance between ^{10}Be and ^{10}B peaks given by

$$\frac{\Delta}{\sqrt{\sigma_{10Be,H}^2+\sigma_{10Be,V}^2+\sigma_{10B,H}^2+\sigma_{10B,V}^2}} \tag{2}$$

where, Δ is the distance between ^{10}Be and ^{10}B peaks, and subscripts H and V mean horizontal and vertical, respectively. Figure 10 shows the experimentally obtained normalized distance with equation (2) as a function of P_C. In the calculation of Equation (2) the value of $\sigma_{10Be,H}$ is substituted in $\sigma_{10B,H}$ for the following two reasons. (i) The precision of $\sigma_{10B,H}$ is inadequate for higher P_C, because the peak of boron becomes so small that the main portion of the peak hides under the lower limit of E_{Res} (0.2 V) as shown in Figure 9. (ii) It has been experimentally observed that the relation $\sigma_{10Be,H} \approx \sigma_{10B,H}$ holds independent of P_C within the range where $\sigma_{10Be,H}$ and $\sigma_{10B,H}$ vary significantly in the same way with P_C. It is found that the values of normalized distance peak at P_C=57 Torr. This is due to the fact that as P_C increases over 55 Torr, the reduction of peak widths becomes saturated, while the distance Δ going into decline because of the enhancement in the energy loss in the gas-cell. It can be said that the optimum P_C is around 57 Torr providing the best discrimination. The nature of the P_C-dependence on the peak-width is attributed to the baseline fluctuation of the pulse trace detected in the ionization chamber, which is briefly discussed in Section 7.

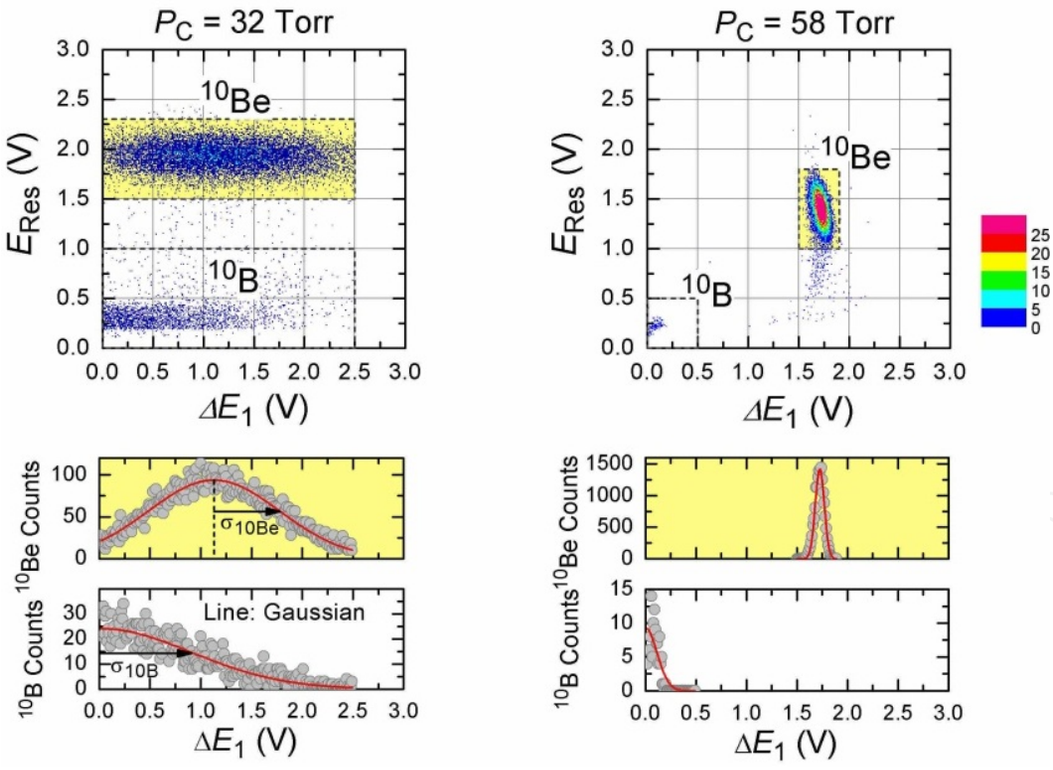

Figure 9. The variation of ΔE_1-E_{Res} spectrum for two gas pressures of the gas-cell, P_C (upper frames). Corresponding peak profiles of ^{10}Be and ^{10}B are also depicted for the ΔE_1 component in the middle and bottom frames, respectively. The peak is fitted by a Gaussian distribution characterized with a standard deviation of σ. The gas pressure for the ionization chamber for left and right cases are 114 Torr and 56 Torr, respectively.

http://dx.doi.org/10.5772/58549

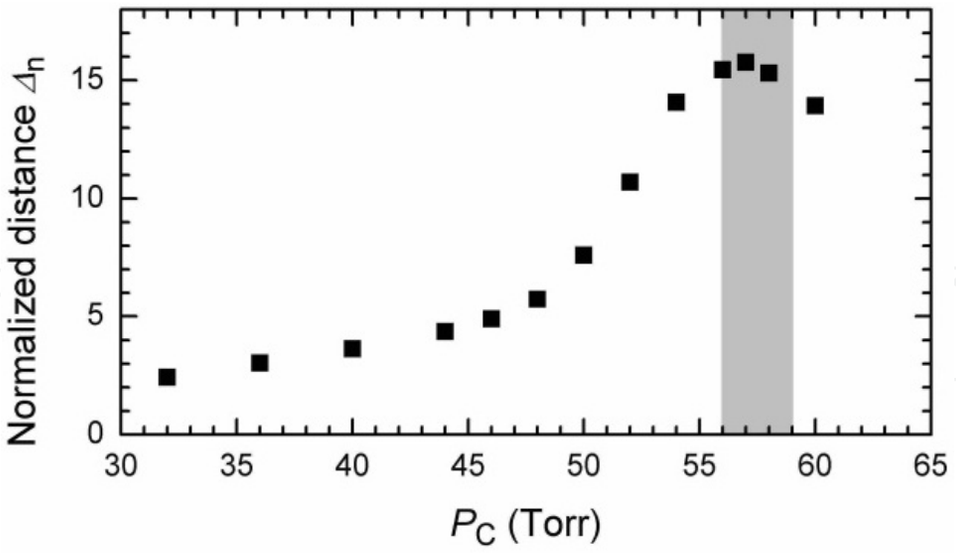

Figure 10. Variation of the normalized distance between ^{10}Be and ^{10}B spectrum peaks as a function of the P_C. The range of P_C indicated by the shaded region is an optimized range, and is usually employed.

5.3. Test measurements, Long-term reliability

We completed the development of the ^{10}Be measurement technique last fiscal year (2012), confirming high stability and reliability of the ^{10}Be/Be ratios in numerous test measurements. Even after we started to perform requested ^{10}Be measurements in 2013, data quality has been continuously checked for every routine measurement using standards. Three typical standards are the ICN standards mention in the Section 5.1, S5-1, S5-2, S6-2, and a blank sample. The blank sample (hereafter BLK) is made from a quantified standard for atomic absorption spectrometry (No.020-07481) produced by Wako Pure Chemical Industries for which a ^{10}Be/Be ratio of ~2×10^{-14} is expected [41]. As shown in Section 5.1, S5-1 is used to obtain the normalization constant given by the measured ratio of S5-1 divided by its nominal ratio. With respect to the data quality of the S5-1 standard, the relative precision, in terms of the relative standard deviation *rsd* is important, since only the *rsd* affects the normalization constant, where the role of the S5-1 standard is similar to that of HOxII standard in the ^{14}C measurement, as described in Section 4.1. The value of *rsd* is around 0.50% for each routine measurement.

Figure 11 shows the quality of measurements from October 2011 to December 2013. The left column shows the evolution of the ^{10}Be/Be ratios using the S5-2, S6-2, and BLK standards. The ^{10}Be measurements have been conducted at intervals ranging from around a few months to half a year. All ^{10}Be/Be ratios for both S5-2 and S6-2 agree with the nominal values within 3σ of each point, where the σ is the combined uncertainty of the counting and the nominal ratio of the S5-1 standard. On the other hand, although the ratio of BLKs lies around its expected range, it seems to vary systematically up and down. This variation can be related to at least two factors: one is beam slit condition, and the other is the problem of the sample preparation. As shown in Figure 11, the time when the BLK ratio is low, in December 2012, coincides with the time when we began to narrow the beam slit behind the ECA to improve the ECA resolu-

tion. The rise in the ratio after December 2012 implies that there could still remain a somewhat unidentified route for contamination in the sample preparation. This interpretation is supported by the observation that the ratio for the commercial, high-purity chemical reagent BeO powder produced by the Mitsuwa Chemical Co., Ltd. stabilized below 10^{-14} after Dec. 2012.

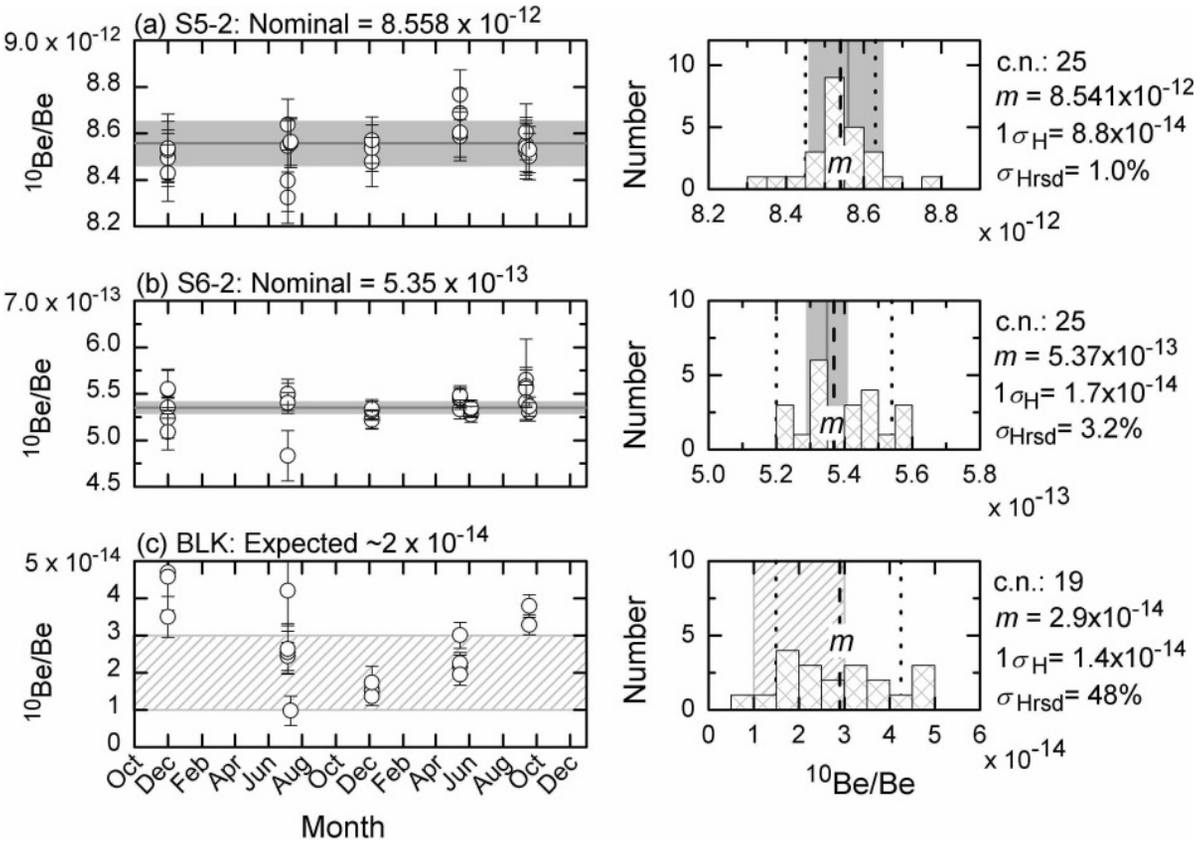

Figure 11. Measurement quality from October 2011 to December 2013 using ^{10}Be-AMS standards: S5-2 (a), S6-2 (b), and blank BLK (c). The left column shows evolution of the measurement results. The gray line and hatching in both the left and right columns depicts respectively the nominal values and their uncertainty. The uncertainty range is based on a nominal uncertainty of 1.1% (1σ) [39]. The right column depicts the corresponding histograms based on the left column measurement points. The dashed and dotted lines represent respectively the mean values (*m*) and their uncertainty ($1\sigma_H$). The symbol c.n. stands for the number of sampling cathodes used in building the histograms, and σ_{Hrsd} is the relative standard deviation of the σ_H.

The frames on the right-hand side of Figure 11 are histograms corresponding to the left-hand frames. It can be seen that the value of *m* (the arithmetic mean of the histogram) for the S5-2 and S6-2 standards are fairly consistent with corresponding nominal values; each difference between measured and nominal value is within the standard deviation of *m*, given by $1\sigma_H/(\text{c.n.})^{0.5}$, i.e., 1.8×10^{-14} for S5-2, and 0.34×10^{-14} for S6-2.

5.4. Comparison test

We performed a comparison test with the AMS system in the MALT using beryllium samples made from an ice core. The samples measured in our system were originally prepared as spares

http://dx.doi.org/10.5772/58549

for the ^{10}Be measurements that had already been performed in the MALT accelerator in 2010. In this test, therefore, the samples measured at both facilities are produced by the same process for the comparison.

Figure 12 and Table 2 show the results of the comparison test. Almost all of the measured ^{10}Be/Be ratios are consistent with the values obtained by the MALT AMS system. There is a significant difference between samples B and H (indicated by the arrow) taking into consideration their uncertainties, which could be due to unknown systematic errors. For the results of the ^{10}Be/Be ratio measured in the MALT AMS system, two data sets are depicted for different data processing methods: one method is used at Hirosaki Univ. Japan, and the other is our method. The algorithms used for drawing the ^{10}Be/Be ratios for both methods are almost the same[1], but the uncertainty has different interpretations, depending on which method is chosen. The uncertainty in the Hirosaki Univ., unc1, represents the standard deviation obtained by repeated measurements, whereas in our method, the uncertainty, unc2, is drawn basically by combining both the counting uncertainty of ^{10}Be and the uncertainty in the nominal value of S5-1 (1.1% for 1σ [39]). The uncertainty in the nominal value affects that in the normalized constant, but is generally not always considered. This is because a lot number of standards does not change until the sample bottle is renewed, and thus the true value of the normalization constant rarely shifts. However, even when one assesses the data quality over a long time frame or performs an inter-laboratory comparison test, one should consider the difference in the lot number in order to accurately compare the isotope ratio values. Despite this fact, as shown in Table 2, there seems to be no systematic difference between unc1 and unc2, as expected. It is noted that the counting uncertainty itself is around 70% of unc1.

Sample	TONO		MALT*			
	Ratio x10^{-12}	unc x10^{-14}	Ratio1 x10^{-12}	unc1 x10^{-14}	Ratio2 x10^{-12}	unc2 x10^{-14}
A	3.278	4.4	3.273	6.4	3.253	6.1
B	6.252	8.0	6.637	14.4	6.617	9.9
C	4.067	5.8	4.095	7.1	4.077	7.4
D	4.406	5.6	4.379	9.3	4.362	7.2
E	2.869	4.1	2.970	9.2	2.951	5.6
F	3.846	5.0	3.967	4.8	3.945	6.1
G	4.501	6.0	4.585	10.0	4.561	7.0
H	4.414	5.6	4.643	5.6	4.620	7.1
I	4.148	5.5	4.266	4.7	4.244	6.8
J	3.618	4.8	3.688	5.7	3.666	6.2

*Ratio1:HIROSAKI Univ., Ratio2: TONO.

Table 2. Results of the comparison test corresponding to the points in Figure 12.

1 In the calculation in the normalized constant, S5-1 and/or S5-2 were used atHirosaki Univ., but only S5-1 was used in the TONO.

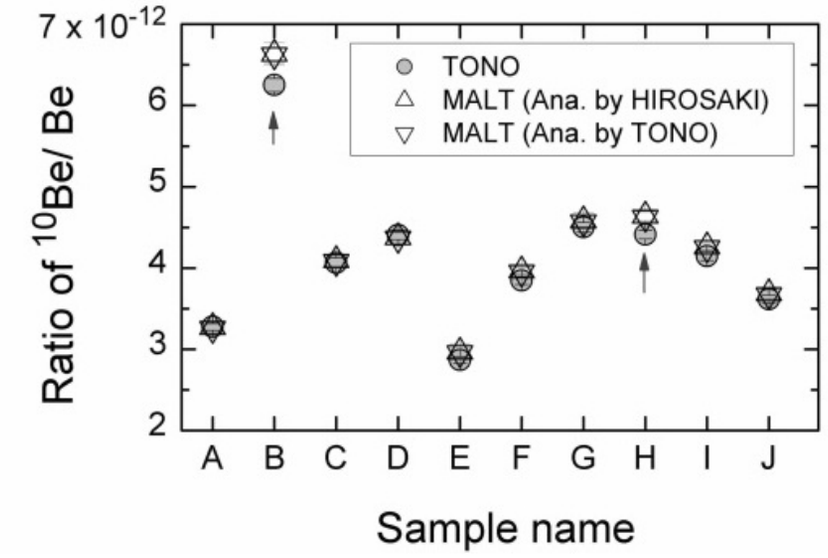

Figure 12. Comparison test using unknown samples.

On the other hand, the average uncertainty for the TONO (unc) is approximately 78% of that for the MALT (unc2). This is due to the fact that the total counts of the ^{10}Be signal for the TONO were three times larger than that for the MALT because of longer measurement time at the TONO. It should be mentioned that the average count rate is 70 cps at the TONO but is 250 cps at the MALT AMS system, a reflection of the different specifications of their respective ion sources. Actually, the ion current for the MALT AMS system can provide a few times larger current than for the TONO.

6. ^{26}Al measurement

6.1. Development and test measurements

Tuning up of the system and the test measurements for the routine ^{26}Al-AMS operation started in March of 2013, after the development of routine ^{10}Be measurements was finished. We plan to complete the development of the routine ^{26}Al-AMS operation in the middle of fiscal year 2014, confirming the long term stability and reliability of the operation through statistical analysis of accumulated data.

For the ^{26}Al measurements, Al_2O_3 powder is chosen as the sample material (mixed with silver powder), and fundamentally no isobar problems occur because ^{26}Mg does not form negative ions. Therefore, the development of the ^{26}Al-AMS procedure is more straightforward than the ^{10}Be-AMS procedure. The configuration for ^{26}Al-AMS is listed in Table 1.

Figure 13 shows the observed $^{26}Al^{3+}$ peak in the E_{Tot}-ΔE_1 spectrum. As described above, there is no other peak. The data points outside the counting gate (the green square) can be attributed to some incident ions reaching the electrode without complete volumetric energy-loss due to large-angle scattering at the window of the ionization chamber.

http://dx.doi.org/10.5772/58549

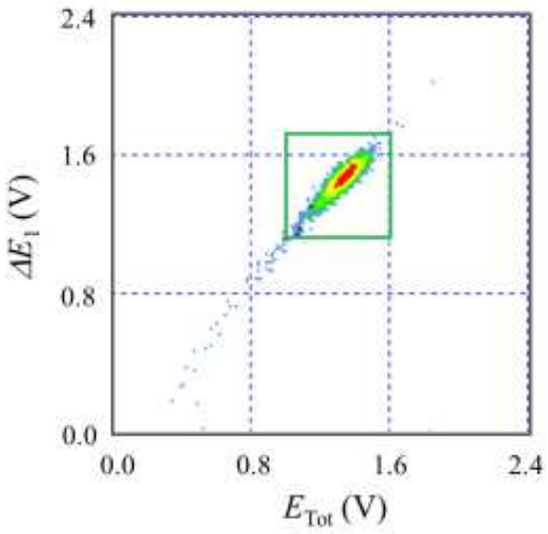

Figure 13. Example of the observed $^{26}Al^{3+}$ peak in the E_{Tot}-ΔE_1 spectrum.

We have performed test measurements using ^{26}Al standards, in order to investigate measurement stability. For the test measurements, the series of standards prepared and distributed by Nishiizumi have been used [42], as well as the ^{10}Be measurement mentioned in Section 5.3. Typical standards, 01-4-1 and 01-5-1 (S4-1 and S5-1, respectively), especially the former have been employed to compute the normalization constant that is given by the measured ratio of a standard S4-1 divided by its nominal ratio. The blank sample (BLK) was made from a quantified standard for atomic absorption spectrometry (No.016-15471) supplied by Wako Pure Chemical Industries.

The left column on Figure 14 shows the results of the two test measurements carried out between routine ^{14}C- and ^{10}Be-AMS operations. Concerning the isotope ratio for the S4-1 standard, only the precision is meaningful (in other words, the accuracy has little meaning), since the arithmetic mean of the points obtained in the same batch (or on same date) is already normalized to the nominal value. A long-term precision can be drawn from the statistical dispersion of the data points displayed on the same figure, which will be mentioned in the below description related to the histogram. All data points for the S5-1 standard are consistent with the nominal value within 3σ, where σ (indicated as error bars) is combined uncertainty from the statistical uncertainty and the uncertainty normalized constant (originated from the uncertainty of the nominal ratio of the S4-1 standard). On the other hand, the result of the BLK implies a decrease in the isotope ratio. This can be due to improvement of the energy resolution of the ECA accomplished by narrowing the beam slit located behind the ECA. It is believed that the contamination to the beamline originates in the ion source or in the high energy beamline where unwanted ions can exist because of the dissociation of molecular ions [5]. Although the expected isotope ratio for the BLK is not yet known, the observed range might be acceptable considering the range of the BLK ratio for ^{10}Be [see Section 5.3].

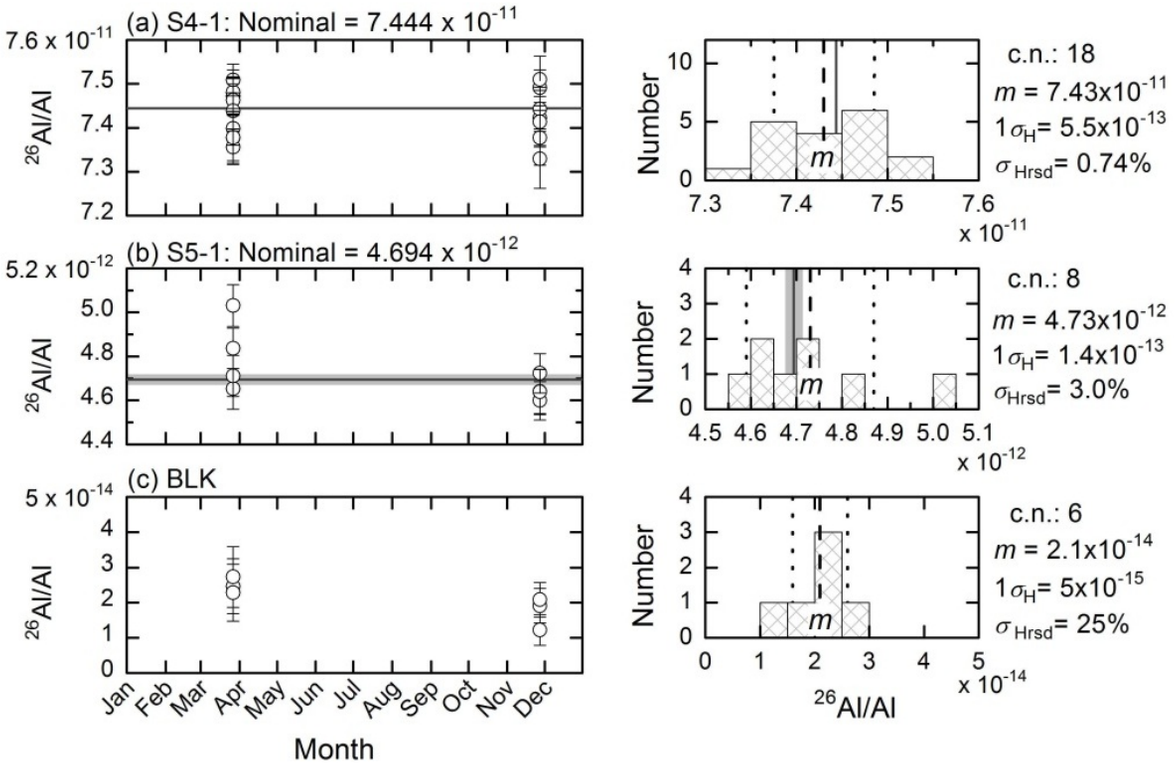

Figure 14. Data quality in test measurements implemented from March 2013 for ^{26}Al standards: S4-1 (a), S5-1 (b), and BLK (c). The left column shows time series plots. The gray line and hatching in (b) for left and right frames indicate the nominal value and the range of its uncertainty, respectively. This range is based on the uncertainty of the absolute value of the nominal value (0.37% for 1σ [42]). The right side shows corresponding histograms representing the left measurements. The dashed and dotted lines stand for arithmetical mean (m) and uncertainty (σ_H), respectively, for the histogram. The symbol c.n. denotes the number of cathodes used for building the histogram, and σ_{Hrsd} is the relative standard deviation of σ_H.

The histograms in the right-side frames in Figure 14 present the data distributions shown as data points in the left-side frames. The long-term precision of the S4-1 standard can be indicated by the statistical dispersion of their points in Figure 14a labelled as σ_H. The relative uncertainty of $\sigma_{H,}$ or σ_{Hrsd} (=0.74%) is less than 0.9%. This magnitude relation, or $\sigma_{Hrsd} < 0.9\%$, provides a necessary condition that the precision of the S5-1 standard would be less than 4% where the value itself is comparable to the precision in the ^{26}Al measurements in the MALT AMS system [18]. Here we assume that the ^{10}Be counts are simply proportional to the nominal ratio, and the S5-1 standard is regarded as representative of ^{26}Al standards except the S4-1 standard. Actually, the nominal ^{26}Al/Al ratio of the S5-1 standard is nearest to a log-average (or a geometric mean) for all the ^{26}Al-AMS standards. As shown in the histogram of the S5-1 standard, the precision is, indeed, less than 4%. Furthermore, the difference between m and the nominal value is less than the standard deviation of the mean given by $\sigma_H/(\text{c.n.})^{0.5}$, indicating there is consistency between them. For all the results shown in this figure, data points are inadequate for a statistical discussion; thus we will need to acquire additional data for evaluation of the measurement stability, in order to develop ^{26}Al routine measurements.

http://dx.doi.org/10.5772/58549

7. Research and development: Baseline fluctuation of the ^{10}Be pulse trace

As described in Section 5.2, we saw that discrimination between ^{10}Be and ^{10}B in the ^{10}Be-AMS is strongly dependent on the gas pressure of the gas-cell (P_C) located in front of gas ionization chamber. The ΔE_1 component of the ^{10}Be peak on the ΔE_1-E_{Res} spectrum shrinks significantly with decreased P_C value. This shrinking, it should be emphasized, accompanies the reduction of the ΔE_1 component of the ^{10}B (see Figure 9), implying the shape of the ^{10}Be peak is closely related to the occurrence of incident ^{10}B, an interfering particle, is briefly discussed.

The peak width is a reflection of the statistical dispersion of the pulse height of signal traces detected from the ionization chamber. Figure 15 shows pulse traces observed by the ΔE_1-electrode for the two P_C values corresponding to Figure 9. One can see that the fluctuation of the baseline of the ^{10}Be signal is greater for the lower P_C. It is noted that there was no remarkable fluctuation in the pulse trace observed by the E_{Res}-electrode; this indicates the dependence of the fluctuation on the distance from the inlet of ionization chamber. In addition, the fluctuation contains frequency components of around a few tenths of a kilohertz. It was observed that the frequency of the major component seems to decrease as P_C increases.

Figure 16 shows both the variation of the standard deviation of the fluctuation (σ in Figure 15) and the energy loss of ^{10}B in the area of ΔE_1, $\Delta E_1{}^{10B}$ (evaluated using SRIM [43]) as a function of P_C. The values of σ and $\Delta E_1{}^{10B}$ decrease in a similar way with increasing P_C, indicating that the fluctuation can be closely related to the incident energy of the ^{10}B.

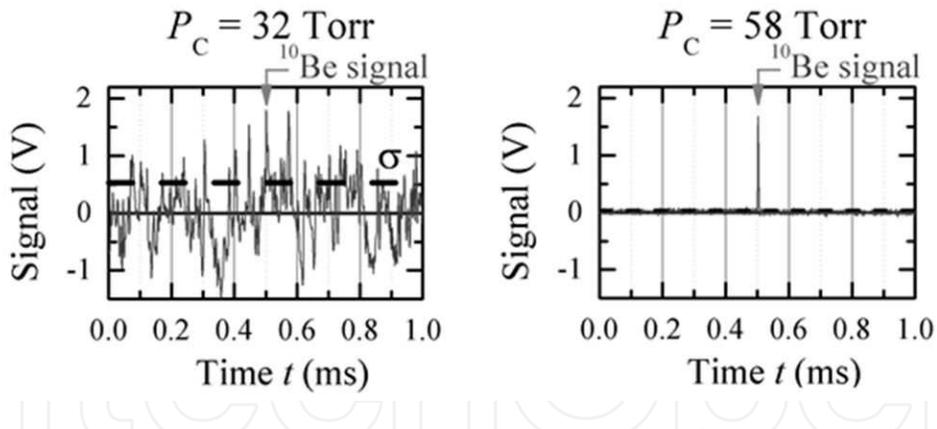

Figure 15. Pulse traces detected by the ΔE_1-electrode in the ionization chamber for two values of P_C corresponding to those shown in Figure 9. The trigger for acquiring the pulse trace is taken from the pulse detected simultaneously by the E_{res}-electrode at t=0.5 ms. The dashed line shows the standard deviation of the fluctuation.

In general, if the incident frequency can no longer be ignored comparing the reciprocal of the time scale for the pulse width, a high counting rate induces pulse pile-up, and deteriorates the time resolution of the ionization chamber. Our investigation, by measuring the ^{10}B current shows that the average frequency of the ^{10}B incident is on the order of a megahertz, which is comparable to the reciprocal of the pulse width. In fact, the amount of ^{10}B entering toward the ionization chamber is expected to be over 10^6 times larger than that of ^{10}Be [40]. The mechanism for the baseline fluctuation, however, is independent of the signal pile-up, but can be due to

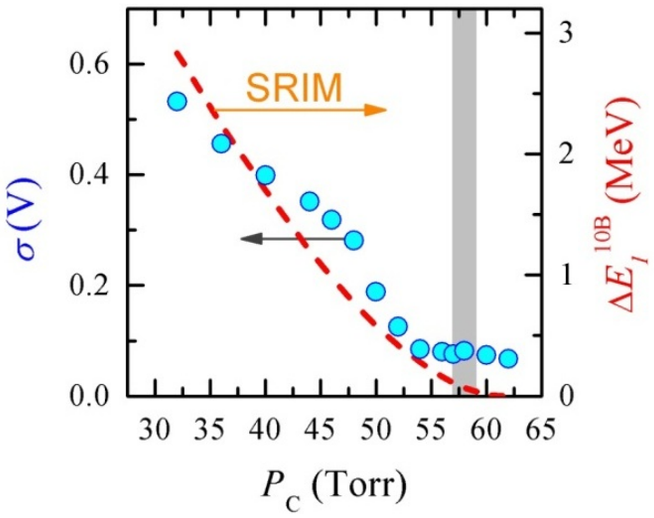

Figure 16. P_C-dependence on the standard deviation of the fluctuation σ. The energy loss of ^{10}B in the ΔE_1 region, ΔE_1^{10B}, deduced by using the SRIM is also shown. The shaded hutch depicts the P_C-range normally used.

the effect of the charge accumulation in the ionization chamber, as qualitatively described below.

In ordinary cases, electrons (negative charges) and ions (positive charges) produced by the ionization caused by the incident ion colliding with atoms in the ionization chamber drift toward the anode and cathode, respectively, in the applied electric field, and finally lose their charge at the electrodes. In the present case, it should be noted that the time interval of the ^{10}B incident is much shorter than the time scale for the ions-loss on the order of milliseconds for the ordinary condition as mentioned above. This can lead to the charge accumulation in the space; the positive charge reaches a certain level so as to provide a balance between production rate and loss rate. The substantial positive charge lowers the anode potential through the inefficiency of the Frisch-grid playing a role in shielding the charges [44,45]. If some instability exists inherently in the relationship between the enhancement of the charge and the ion loss system, the anode potential, therefore, can fluctuate around its equilibrium value. Volumetric ion-electron recombination would be a candidate system for causing an instability so as to enhance the fluctuation of positive charge. This kind of degradation of the performance of the ionization chamber caused by the residual positive charge is not just related to the ^{10}Be measurement, but to more general measurements of rare isotopes accompanied by the isobar problem. Indeed, an effect of remaining charge was mentioned in a paper for improving the discrimination of ^{36}S in ^{36}Cl-AMS [46]. Therefore, it can be said that the investigation of the nature of pulse trace presented here has been conducted as a preparatory activity in the development of the ^{36}Cl-AMS operation.

8. Summary

The AMS system operating at the Tono Geoscience Center (TGC) has not only continued to contribute reliable routine AMS measurements, but also made steady progress in developing

http://dx.doi.org/10.5772/58549

multi-nuclide AMS in order to provide geochronological dating methods applicable to the entire Quaternary timescale.

Our versatile AMS system, based on the 5 MV Pelletron™ tandem accelerator, is designed for AMS analysis of most radio-isotopes including ^{10}Be, ^{14}C, ^{26}Al, ^{36}Cl, and ^{129}I. The AMS system is in good condition after fifteen years of operation, ensured by regularly scheduled maintenance. Total measurement time has been increasing for the last 15 years, and reached 15,000 hours this year. The average annual number of samples measured is 800, and the grand total number of samples will exceed 12,500 within a few months.

In the ^{14}C-AMS operation, the long-term reliability of routine measurements has been continuously verified by measuring standard samples such as C1, C5, and so on, produced by the IAEA, and HOxII produced by the NIST and by comparative testing with other AMS facilities. Almost all the relative standard deviations of the isotope ratios of HOxII in percent modern carbon are less than 0.25% for each measurement, and the average isotope ratio of C1 lies around 0.15 pMC. The comparison tests were carried out twice, in 2010 and in 2012, with the AMS facility at the JAEA-AMS-MUTSU. The results showed that there was no significant difference in the data obtained from the facilities.

With respect to the ^{10}Be-AMS operation, we completed the development of ^{10}Be measurement capability last year, confirming both high stability and reliability of the ^{10}Be/Be ratios obtained from numerous test measurements. Then, routine measurements started since the beginning of fiscal year 2013. The detection limit of the isotope ratio can be less than 7×10^{-15}, estimated by using samples made of commercial high-purity BeO powders. For the development of ^{10}Be-AMS, discrimination of ^{10}Be from ^{10}B was accomplished by optimization of gas pressure in the gas cell located in front of gas ionization chamber. We also performed a comparison test with the AMS system at the MALT in the University of Tokyo using beryllium samples taken from an ice core. Measured ^{10}Be/Be ratios were consistent with the values obtained by the MALT group, confirming the reliability of our measurements.

We have now entered into the development of ^{26}Al-AMS. This development and the test measurement have progressed and have shown satisfactory results. We have performed system tuning and test measurements using ^{26}Al standard samples. Almost all measured ratios of ^{26}Al/Al are consistent with nominal values, within the range of their uncertainty and routine measurements of ^{26}Al will start in the near future.

We have also conducted investigations for improving the heavy ion detection system based on the ΔE-E_{Res} type-gas ionization chamber with multi-anodes. It has been observed that the high incident ion rate of the stable isobars into the gas ionization chamber disturbs the baseline of the pulse trace for the measured rare nuclide. This can be related to the fact that the remaining positive charge produced by isobars makes the anode signal fluctuate, which will be one of key factors that should be resolved for achieving the ^{36}Cl-AMS with good discrimination of ^{36}S, a stable isobar. The development for the ^{36}Cl-AMS analysis will be one focus for development work in the next few years.

Acknowledgements

We would like to express our gratitude to Prof. Matsuzaki of the University of Tokyo for his continuous academic and practical advice. We would like to offer our special thanks also to Dr. Horiuchi of Hirosaki University for providing unknown beryllium samples and measurement data. Special thanks to Mr. Hanaki of the facility administrator for his management support and constant encouragement. We also thank the staff members of the AMS laboratory for their help and support.

Author details

Akihiro Matsubara[1*], Yoko Saito-Kokubu[1], Akimitsu Nishizawa[2], Masayasu Miyake[2], Tsuneari Ishimaru[1] and Koji Umeda[1]

*Address all correspondence to: matsubara.akihiro@jaea.go.jp

1 Tono Geoscience Center, Japan Atomic Energy Agency, Jorinji, Izumi, Toki, Japan

2 Pesco Corp., Ltd., Tokiguchiminami, Toki, Japan

References

[1] GIRDD. Geological Isolation Research and Development Directorate (GIRDD). Available: http://www.jaea.go.jp/04/tisou/english/index/e-index.html. Accessed 5 January 2014.

[2] Asamori K, Niwa M, Hanamuro T, Yamada K, Kusano T, et al. Annual Report for Research on Geosphere Stability for Long-Term Isolation of Radioactive Waste in Fiscal Years 2011. JAEA-Research 2012; 24.

[3] Yasue K, Asamori K, Niwa M, Hanamuro T, Saito-Kokubu Y, et al. Research Plan on Geosphere Stability for Long-Term Isolation of Radioactive Waste (Scientific Programme for Fiscal Year 2013). JAEA-Review 2013; 023.

[4] Finkel RC, Suter M. AMS in the Earth Sciences: Technique and Applications. Advances in Analytical Geochemistry; 1993: 1-114.

[5] Tuniz C, Bird JR, Fink D, Gregory F H. Accelerator Mass Spectrometry: Ultrasensitive Analysis for Global Science. CRC Press; 1998.

[6] Muzikar P, Elmore D, Granger DE. Accelerator mass spectrometry in geologic research. Geological Society of America Bulletin 2003; 115: 643–654.

[7] IVY-OCHS S, KOBER F. Surface exposure dating with cosmogenic nuclides. Quaternary Science Journal (Eiszeitalter und Gegenwart) 2008; 57: 179–209.

[8] Asamori K, Niwa M, Hanamuro T, Yamada K, Kusano T, et al. Annual Report for Research on Geosphere Stability for Long-Term Isolation of Radioactive Waste in Fiscal Years 2012. JAEA-Research 2014; in press.

[9] Xu S, Ito S, Iwatsuki T, Abe M, Watanabe M. A new AMS facility at the JNC Tono Geoscience Center, Japan. Nuclear Instruments and Methods in Physics Research Section B: Beam Interactions with Materials and Atoms 2000; 172: 8–12.

[10] Itoh S, Abe M, Watanabe M, Nakai S, Touyama H, et al. Present status of the JNC Tono Geoscience Center AMS system. Nuclear Instruments and Methods in Physics Research Section B: Beam Interactions with Materials and Atoms 2004; 223-224: 100–103.

[11] Saito-Kokubu Y, Nishizawa A, Suzuki M, Ohwaki Y, Nishio T, et al. Current status of the AMS facility at the Tono Geoscience Center of the Japan Atomic Energy Agency. Nuclear Instruments and Methods in Physics Research Section B: Beam Interactions with Materials and Atoms 2013; 294: 43–45.

[12] Matsubara A, Kokubu Y, Nishizawa A, Owaki Y, Nishio T, et al. Current status of JAEA-AMS-TONO, the Japan Atomic Energy Agency (2011). 4th East Asian Symposium on Accelerator Mass Spectrometry (EA-AMS-4). Tokyo. pp. 147–150.

[13] Matsubara A, Saito-Kokubu Y, Nishizawa A, Miyake M, Ishimaru T. System technology for ^{10}Be and ^{26}Al measurements in the JAEA-AMS-TONO (2013). 5th East Asia AMS Symposium (EA-AMS-5). Daejeon. p. 53.

[14] Saito-Kokubu Y, Ishimaru T, Matsubara A, Nishizawa A, Miyake M, et al. Present status of JAEA-AMS-TONO; Progress of multi nuclide AMS (2013). 5th East Asia AMS Symposium (EA-AMS-5). Daejeon. p. 22.

[15] Matsubara A, Nishizawa A, Miyake M, Saito-Kokubu Y, Ishimaru T. Development of System Techonology for Routine ^{10}Be Measurement in the JAEA-AMS-TONO (in Japanese) (2013). Proceedings of the 15th Japaneses Symposium on Accelerator Mass Spectrometry. Nagoya. pp. 25–28.

[16] JAEA. Procedure of shared use of JAEA facilities. Available: http://sanga-ku.jaea.go.jp/3-facility/05-support/jaea-facilities-eng.html. Accessed 8 January 2013.

[17] Sundquist M. 15SDH-2 AMS SYSTEM MANUAL. National Electrostatics Corp.; 1998.

[18] Matsuzaki H, Nakano C, Tsuchiya Y (Sunohara), Kato K, Maejima Y, et al. Multi-nuclide AMS performances at MALT. Nuclear Instruments and Methods in Physics Research Section B: Beam Interactions with Materials and Atoms 2007; 259: 36–40.

[19] Kume H, Shibata Y, Tanaka A, Yoneda M, Kumamoto Y, et al. The AMS facility at the National Institute for Environmental Studies (NIES), Japan. Nuclear Instruments

and Methods in Physics Research Section B: Beam Interactions with Materials and Atoms 1997; 123: 31–33.

[20] Xu S, Anderson R, Bryant C, Cook G. Capabilities of the new SUERC 5MV AMS facility for 14C dating. Radiocarbon 2004; 46: 59–64.

[21] Maden C, Anastasi P.A.F., Dougans A, Freeman S.P.H.T., Kitchen R, et al. SUERC AMS ion detection. Nuclear Instruments and Methods in Physics Research Section B: Beam Interactions with Materials and Atoms 2007; 259: 131–139.

[22] Alfimov V, Possnert G, Aldahan a. Measurements of ^{36}Cl with a gas-filled magnet at the Uppsala tandem laboratory. Nuclear Instruments and Methods in Physics Research Section B: Beam Interactions with Materials and Atoms 2007; 259: 199–203.

[23] Salehpour M, Håkansson K, Possnert G. Accelerator mass spectrometry of ultrasmall samples with applications in the biosciences. Nuclear Instruments and Methods in Physics Research Section B: Beam Interactions with Materials and Atoms 2013; 294: 97–103.

[24] Stocker M, Döbeli M, Grajcar M, Suter M, Synal H-A, et al. A universal and competitive compact AMS facility. Nuclear Instruments and Methods in Physics Research Section B: Beam Interactions with Materials and Atoms 2005; 240: 483–489.

[25] Kerver S. Compact Universal AMS (UAMS) Systems. Available: http://www.pelletron.com/compactams.htm. Accessed 8 January 2014.

[26] Hong W, Hun J, Ki P, Sung S, Joo H, et al. A New 1MV AMS Facility at KIGAM. Raiocarbon 2010; 52: 243–251.

[27] Matsubara A, Nishizawa A, Suzuki M, Owaki Y, Nishio T, et al. Improvements of the JAEA-AMS-TONO; FY2009 (2010). 23th Proceedings of research workshop on tandem accelerator and its related technology (in Japanese). Tokyo. pp. 53–56.

[28] Southon JR, Santos GM. Ion Source Development at KCCAMS, University of California, Irvine. Radiocarbon 2004; 46: 33–39.

[29] Travertine M, Wood C, Sucrose W. Reference Sheet for Quality Control Materials. Available: http://nucleus.iaea.org/rpst/Documents/rs_IAEA-C1_to_IAEA-C9.pdf.

[30] "abc" NEC AMS Analysis Program, Version 6.1. National Electrostatics Corp.; 2005.

[31] Stenström KE, Skog G, Georgiadou E, Genberg J, Johansson A. A Guide to Radiocarbon Units and Calculations. LUNFD6 2011; 6: 1–17.

[32] Xu X, Khosh M, Druffel-Rodriguez K, Trumbore S, Southon J. Is the Consensus Value of ANU Sucrose (IAEA C-6) Too High? Radiocarbon 2010; 52: 866–874.

[33] Sato M, Itoh S, AHN S, Hirota M, Yamagata H, et al. Current status of the Compact AMS system at Paleo Labo Co., Ltd. (2013). Proceedings of the 15th Japaneses Symposium on Accelerator Mass Spectrometry. Nagoya. pp. 17–20.

[34] Kobayashi K, Niu E, Itoh S, Yamagata H, Lomtatidze Z, et al. The compact ^{14}C AMS facility of Paleo Labo Co., Ltd., Japan. Nuclear Instruments and Methods in Physics Research B 2007; 259: 31–35.

[35] Aramaki T, Mizushima T, Mizutani Y, Yamamoto T, Togawa O, et al. The AMS facility at the Japan Atomic Energy Research Institute (JAERI). Nuclear Instruments and Methods in Physics Research Section B: Beam Interactions with Materials and Atoms 2000; 172: 18–23.

[36] Kabuto S, Kinoshita N, Tanaka T, Yamamoto N. Operational Status of the JAEA-MUTSU Tandetron AMS 2008-2009. Prosceedings of the Second JAEA Tandetron AMS Utilization Workshop: November 12-13, 2009, Mutsu-shi, Japan. JAEA. pp. 126–129.

[37] Imamura M, Hashimoto Y, Yoshida K, Yamane I, Yamashita H, et al. Tandem Accelerator Mass Spectrometery of $^{10}Be/^{9}Be$ with Internal Beam Monitor Method. Nuclear Instruments and Methods in Physics Research B 1984; 5: 211–216.

[38] Matsuzaki H, Tanikawa M, Kobayashi K, Hatori S. Development of a gas counter for AMS measurement of ^{10}Be and ^{26}Al of cosmic spherules. Nuclear Instruments and Methods in Physics Research B 2000; B 172: 218–223.

[39] Nishiizumi K, Imamura M, Caffee MW, Southon JR, Finkel RC, et al. Absolute calibration of ^{10}Be AMS standards. Nuclear Instruments and Methods in Physics Research Section B: Beam Interactions with Materials and Atoms 2007; 258: 403–413.

[40] Grajcar M. New concepts of ^{10}Be Accelerator Mass Spectrometry at low energies. Swiss Federal Institute of Technology; 2005.

[41] Horiuchi K, Oniyanagi I, Wasada H, Matsuzaki H. ^{10}Be measurements at MALT using reduced-size samples of bulk sediments. Nuclear Instruments and Methods in Physics Research Section B: Beam Interactions with Materials and Atoms 2013; 294: 72–76.

[42] Nishiizumi K. Preparation of ^{26}Al AMS standards. Nuclear Instruments and Methods in Physics Research Section B: Beam Interactions with Materials and Atoms 2004; 223-224: 388–392.

[43] Ziegler JF, Ziegler MD, Biersack JP. SRIM – The stopping and range of ions in matter (2010). Nuclear Instruments and Methods in Physics Research Section B: Beam Interactions with Materials and Atoms 2010; 268: 1818–1823.

[44] Bunemann O, Cranshaw TE, Harvey JA. Design of grid ionization chambers. Canadian Journal of Research 1949; 27: 191–206.

[45] Al-Adili A, Hambsch F-J, Bencardino R, Oberstedt S, Pomp S. Ambiguities in the grid-inefficiency correction for Frisch-Grid Ionization Chambers. Nuclear Instruments and Methods in Physics Research A 2012; 673: 116–121.

[46] Martschini M, Andersson P, Forstner O, Golser R, Hanstorp D, et al. AMS of ^{36}Cl with the VERA 3MV tandem accelerator. Nuclear Instruments and Methods in Physics Research Section B: Beam Interactions with Materials and Atoms 2013; 294: 115–120.

IntechOpen